J|A|C|S
ARTICLES
Published on Web 12/28/2002

Templating and Supersaturation-Driven Anti-Templating: Principles of Biomineral Architecture

Xiang Y. Liu* and See Wai Lim

Contribution from the Department of Physics, Faculty of Science, National University of Singapore, 2 Science Drive 3, Singapore 117542

Received March 8, 2002; E-mail: phyliuxy@nus.edu.sg

Abstract: The structural synergy between biominerals ($CaCO_3$, hydroxyapatite) and biosubstrates were examined for the first time. The templating effect of substrate and a newly identified *supersaturation-driven interfacial structure mismatch effect* were identified in the context of a new nucleation model. It follows that the heterogeneous nucleation which corresponds to a good structural match and synergy between biominerals and substrates will promote an ordered, compact, and tough complex biomineral structure, and occur only at low supersaturations, whereas at high supersaturations the heterogeneous nucleation associated with a poor structural match and synergy between biominerals and substrates will become dominant due to supersaturation-driven interfacial structural mismatch. The latter normally results in a disordered and porous structure. A phenomenon, so-called microgravity-driven homogeneous nucleation, was also examined. It turns out that microgravity will suppress convection and consequently promote homogeneous-like nucleation during biomineralization. This could be responsible for microgravity-induced osteoporousis.

Introduction

Biological mineralization and demineralization play a vital part in our life and the environment around us. The mechanism of formation of minerals in biological systems raises a number of questions, which still await satisfactory answers. Teeth and hard tissues consist of different inorganic materials composed mainly of hydroxyapatite (HAP, $Ca_{10}(PO_4)_6(OH)_2$) and organic materials or matrices. The hydroxyapatite crystallites are preferentially packed and aligned cooperatively between the organic materials and matrices.[1−3] The structural synergy between hydroxyapatite and organic substrates determines the unique and amazing elastic and mechanical properties of hard tissues. In nature, some plants and animals utilize Ca minerals to fabricate various hard tissues with a broad range of patterns and properties in terms of organic matrices, such as mollusc shells. However, the way biometrics guide the building up of nanosized biominerals in hard tissues remains an open question.[4]

Our goal is to obtain a fundamental understanding of the controlling mechanism of bioorganic materials and matrices during biomineralization/demineralization so that new techniques can be identified to control the regeneration of hard tissues which ensures that the resulting bionanostructure and mechanical properties will be the same as or very similar to those of the natural one.

In this work, we will examine in the context of Ca mineral nucleation the effects of the biosubstrate, supersaturation, and microgravity on the micro/nanostructure correlation between substrate and biominerals and their implications in hard tissue formation. Moreover, we will focus on the nucleation of hydroxyapatite and $CaCO_3$. Because $CaCO_3$ occurs abundantly in biomineralizing systems[5] and crystallizes easily, it has emerged as a model crystal for establishing understanding of the process of biomineralization[5−13]

Effect of Nucleation Kinetics on Biomineral/Substrate Interface Structural Correlation

In this section, we will examine the effect of substrate on the nucleation of biominerals from the point of view of nucleation kinetics.

A. Model of Heterogeneous Nucleation. It has been generally believed that heterogeneous nucleation is dominant at low supersaturations,[12−16] whereas homogeneous nucleation occurs at high supersaturations.[14,15] Recent progress in nucleation

(1) Anderson, H. C. *J. Cell Biol.* **1969**, *41*, 59−72.
(2) Ali, S. Y.; Evens, L. *Biochem. J.* **1973**, *134*, 647.
(3) Ten Cate, A. R. *Oral Histology: Development, Structure and Function*; Mosby: St. Louis, 1985.
(4) Arends, J. In *Biological Mineralization and Demineralization*; Nancollas, G. H., Ed.; Springer-Verlag: Berlin, 1982; pp 303−324.
(5) Berman, A.; Addadi, L.; Weiner, S. *Nature* **1988**, *331*, 546−548.
(6) Mann, S. *Nature* **1993**, *365*, 499−505.
(7) Mann, S.; Archibald, D. D.; Didymus, J. M.; Douglas, T.; Heywood, B. R.; Meldrum, F. C.; Reeves, N. J. *Science* **1993**, *261*, 1286−1292.
(8) Belcher, A. M.; Wu, X. H.; Christensen, R. J.; Hansma, P. K. *Nature* **1996**, *381*, 56−58.
(9) Teng, H. H.; Dove, P. M. *Am. Mineral.* **1997**, *82*, 878.
(10) Walters, D. A.; Smith, B. L.; Belcher, A. M.; Paloczi, G. T.; Stucky, G. D.; Morse, D. E.; Hansma P. K. *Biophys. J.* **1997**, *72*, 1425−1433.
(11) Sikes, C. S.; Yeung, M. L.; Wheeler, A. P. In *Discovery and Commercialization*; Sikes, C. S., Wheeler, A. P., Eds.; American Chemical Society: Washington, DC, 1991; pp 50−71.
(12) Chernov, A. A. *Modern Crystallography III: Crystal Growth*; Springer-Verlag: Berlin, 1984.
(13) Chayen, N. E. *J. Appl. Crystallogr.* **1997**, *30*, 198−203.
(14) Nielsen, A. E.; Christofferesen, J. In *Biological Mineralization and Demineralization*; Nancolllas, G. H., Konferenzen, D., Eds.; Springer-Verlag: Berlin, 1982; pp 37−77.
(15) Skripov, V. P. In *Current Topics in Materials Science*, 2nd ed.; Kaldis, E., Scheel, H. J., Eds.; North-Holland: Amsterdam, 1977; pp 327−378.

10.1021/ja020355d CCC: $25.00

studies[17,18] suggests an alternative explanation for these results. If the interfacial free energy between the crystal and the fluid phase is not too low, nucleation is normally controlled by a number of heterogeneous nucleation processes as supersaturation increases.

Let us look at the general nucleation process: the constituent molecules or ions in the solution may, on collision, join into groups of two or more particles to form dimers, trimers, tetramers, and so forth. Before the embryos can reach a critical radius, r_c, they are unstable even when a positive thermodynamic driving force $\Delta\mu$ is applied. To reach r_c, an energy barrier, the so-called nucleation barrier, needs to be overcome. In which way and at which number the embryos reach the critical radius is the main concern. When the nucleation barrier is overcome, the second stage of the phase transition begins: growth.

In the process of nucleation, increase in the size of an embryo should overcome a free energy barrier, so-called nucleation barrier, ΔG^*, for a given $\Delta\mu$ ($\Delta\mu$: chemical potential difference between the actual state and the equilibrium state) before it can become a stable growing crystal in the system. In the case of homogeneous nucleation, the effect of the substrate is negligible. The nucleation barrier is then given for a spherical nucleus by[12−15,19,20]

$$\Delta G^*_{\text{homo}} = \frac{16\pi\gamma_{\text{cf}}{}^3\Omega^2}{3[\Delta\mu]^2} \tag{1}$$

and the critical size of the nuclei is

$$r_c = 2\gamma_{\text{cf}}/\Delta\mu \tag{2}$$

$$\Delta\mu = kT\ln(1+\sigma) \tag{3}$$

where ΔG^*_{homo} is the nucleation barrier for homogeneous nucleation, k is the Boltzmann constant, T is the absolute temperature, and Ω is the volume of the growth unit. In the equation, σ is defined as the supersaturation of solution, and for $CaCO_3$, one has

$$\ln(1+\sigma) = \ln[a(Ca^{2+})a(CO_3{}^{2-})/K_{\text{sp}}] \tag{4}$$

and for HAP

$$\ln(1+\sigma) = \ln\{[a(Ca^{2+})]^{10}[a(PO_4{}^{3-})]^6[a(OH^-)]^2/K_{\text{sp}}\} \tag{5}$$

where K_{sp} is the solubility product at a given temperature (in our case, $T = 25$ °C) and $a(i)$ is the activity of species i.

In the presence of substrates with an average radius of R^s (cf. Figure 1a), the nucleation barrier is then reduced to

$$\Delta G^* = \Delta G^*_{\text{homo}} f\ [0 \le f \le 1] \tag{6}$$

We will derive the expression of f as follows (see Figure 1). As shown in Figure 1a, we assume that nucleation occurs at a substrate with a radius of R^s. The mother phase is represented by subscript f, the cluster of the crystalline phase by c and the substrate by s. If we denote volume by V and surface area of the substrate by S, the free energy of formation of a cluster of radius r on a foreign particle of radius R^s is given by

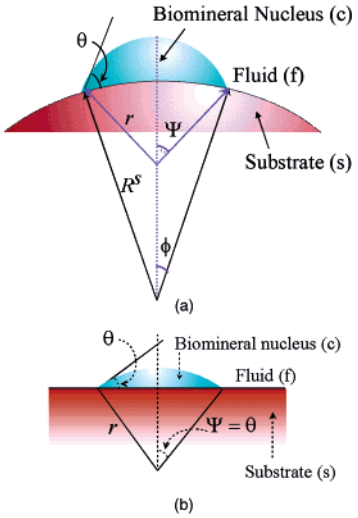

Figure 1. (a) Schema showing the nucleation of biominerals on a substrate with the radius of curvature R^s. (b) Schematic illustration for the nucleation of biominerals on a flat substrate ($R^s \to \infty$, $\phi \to 0$, $\psi = \theta$).

$$\Delta G = -\Delta\mu V_s/\Omega + \gamma_{\text{cf}}S_{\text{cf}} + (\gamma_{\text{sc}} - \gamma_{\text{sf}})S_{\text{sc}} \tag{7}$$

where γ_{ij} is the surface free energy between phases i and j and Ω is the volume per structural unit. Assume that the concept of contact angle can still be applied in this case. We have then

$$m = (\gamma_{\text{sf}} - \gamma_{\text{sc}})/\gamma_{\text{cf}} \approx \cos\theta, \quad (-1 \le m \le 1) \tag{8}$$

Referring again to Figure 1a, we have

$$S_{\text{sc}} = 2\pi(R^s)^2(1-\cos\phi), \quad S_{\text{cf}} = 2\pi r^2(1-\cos\psi) \tag{9}$$

and

$$V_s = \frac{1}{3}\pi r^3[2-(3\cos\psi)+\cos^3\psi] - \frac{1}{3}\pi(R^s)^3[2-(3\cos\phi)+\cos^3\phi] \tag{10}$$

with

$$\cos\phi = \frac{R^s - (r\cos\theta)}{l} = \frac{R^s - rm}{l} \tag{11}$$

$$\cos\psi = \frac{-[r-(R^s\cos\theta)]}{l} = \frac{-(r-R^sm)}{l} \tag{12}$$

and

$$l = [(R^s)^2 + r^2 - 2R^srm]^{1/2} \tag{13}$$

To evaluate the critical free energy $\Delta G^*_{\text{heter}}$, we require that

$$(\partial\Delta G/\partial r) = 0 \tag{14}$$

Regarding the fact that the radius of curvature r_c of the critical nuclei is determined by γ_{cf} and the driving force

(16) Malkin, A. I.; Chernov, A. A.; Alexeev, I. V. *J. Crystal Growth* **1989**, *97*, 765−769.
(17) Liu, X. Y. *J. Chem. Phys.* **1999**, *111*, 1628−1635.
(18) Liu, X. Y.; Strom, C. S. *J. Chem. Phys.* **2000**, *113*, 4408−4411.

$\Delta\mu$,[12,21] we then have

$$r_c = 2\Omega\gamma_{cf}/\Delta\mu = 2\Omega\gamma_{cf}/kT\ln(1+\sigma) \quad (15)$$

We notice that in the case of epitaxial growth, the structural mismatch at the crystal−substrate interface will give rise to the strain, which affects both the bulk free energy of nuclei and the interfacial free energy γ_{cf}. In this case, the occurrence of substrate exerts an impact on r_c. Nevertheless, in many cases, such as the nucleation of biominerals on soft biological substrates, the strain is very low. Therefore, its effect on r_c is neglected in our treatment.

Substituting expressions 8−15 into eq 7 gives rise to

$$R' = \frac{R^s}{r_c} = \frac{R^s\Delta\mu}{\Omega\gamma_{cf}} = \frac{R^s kT\ln(1+\sigma)}{\Omega\gamma_{cf}} \quad (16)$$

The free energy of formation of critical nucleus is given by eqs 6 and 1

$$f = f(m,R') = \frac{1}{2} + \frac{1}{2}\left(\frac{1-mR'}{w}\right)^2 + \frac{1}{2}R'^3\left[2 - 3\left(\frac{R'-m}{w}\right) + \left(\frac{R'-m}{w}\right)^2\right] + \frac{3}{2}mR'^2\left(\frac{R'-m}{w} - 1\right) \quad (17)$$

and

$$w = [1 + (R')^2 - 2R'm]^{1/2} \quad (18)$$

Here R' is actually the dimensionless radius of curvature of the substrate with reference to the radius of critical nuclei r_c. In other words, it only makes a generic sense if the curvature of the substrate is referred to the curvature of critical nuclei. $f(m,R')$ occurring in eq 6 describes the lowering of the nucleation barrier due to the presence of the substrate. Evidently, $f(m,R')$ in the exponential term describes the reduction of the nucleation barrier from a genuine homogeneous nucleation G^*_{homo} to the actual heterogeneous nucleation ΔG^*.

If $R^s \to \infty$, the substrate is essentially a flat surface, and $\psi = \theta$, and $\phi = 0$. In this case, $R' \to \infty$, and $f(m,R')$ becomes $f(m)$, a solo function of m. Under this condition, S_{sc}, S_{cf}, and V_s given by eqs 9 and 10 can be simplified as

$$S_{sc} = \pi r^2[1 - (\cos\theta)^2], \quad S_{cf} = 2\pi r^2(1-\cos\theta) \quad (9')$$

and

$$V_s = \frac{1}{3}\pi r^3(2+\cos\theta)(1-\cos\theta)^2 \quad (10')$$

Substituting eq 9′ and eq 10′ into eq 7 and repeating step 14, $f(m)$ can be obtained on the basis of the definitions 6 and 8, as

$$f(m) = \frac{1}{4}(2+m)(1-m)^2 = \frac{1}{4}(2-3m+m^3) \quad (19)$$

Taking into account the effect of the substrate on both the nucleation barrier and the transport process, the nucleation rate is given by[17]

$$J = (R^s)^2 N^\circ f''(m,R')[f(m,R')]^{1/2} B \exp\left[-\frac{\Delta G^*_{homo}}{kT} f(m,R')\right] \quad (20)$$

with

$$f''(m,R') = \frac{1 + (1-R'm)/w}{2} \quad (21)$$

and

$$f(m,R') = f(m) = \frac{1}{2}(1-m) \quad \text{at } R' \gg 1 \quad (22)$$

where B is the kinetic constant and N° denotes the density of substrates (or "seeds").

Both $f(m,R')$ and $f''(m,R')$ are functions of m and R'. When $R' \to 0$ or $m = -1$, $f(m,R')$, $f''(m,R') = 1$. This is equivalent to the case of homogeneous nucleation. In the case where $m \to 1$ and $R' \gg 1$, one has $f(m,R')$, $f''(m,R') = 0$. Normally, heterogeneous nucleation occurs in the range of m between 1 and −1, or $f(m,R')$ between 0 and 1, depending on the nature of the substrate surface and supersaturation.

To describe the kinetics of nucleation, one of the most common ways is to measure the induction time of nucleation at different supersaturations.

By definition, one has

$$J = 1/(t_s V) \quad (23)$$

where V is the volume of the system. Denoting the induction time for nucleation of the steady state t_s, it follows then from eq 20 that

$$\ln t_s = \frac{\kappa}{[\ln(1+\sigma)]^2} f(m,R') - \ln[V(R^s)^2 N^\circ f''(m,R')[f(m,R')]^{1/2} B] \quad (24)$$

with

$$\kappa = \frac{16\gamma_{cf}^3\Omega^2}{3(kT)^3} \quad (25)$$

B. Effects of Template and Supersaturation-Driven Interfacial Structural Mismatch. In the case where the radius of curvature of substrate is not too small, r_c can be much smaller than R^s at relative high supersaturations. According to eq 16, this situation gives rise to a large R'. In the case where $R' \gg 1$, the substrate can be regarded as essentially flat. In this case, $f(m,R') = f(m)$ is then dependent only on m, and independent of supersaturation (eqs 2, 3, 6, 16, and 17). We will focus our attention on this case. Note that for biomineralization,[16] substrate refers to any biosubstrate, including biomatrices and/or existing biomineral crystallites.[17,18]

As given by eq 8, m is directly associated with γ_{cs}, which is determined by the interaction and/or structural match between the crystalline phase and the substrate. For a given crystalline phase and a substrate, an optimal structural match is the crystallographic orientation $\{hkl\}$, corresponding to the strongest *average* interaction or the lowest interfacial energy difference between the crystalline phase and the substrate between the two

(19) Söhnel, O.; Mullin, J. W. *J. Crystal Growth* **1978**, *44*, 377−382.
(20) Söhnel, O.; Mullin, J. W. *J. Colloid Interfac. Sci.* **1988**, *123*, 43−50.
(21) Mullin, J. W. *Crystallisation*; Butterworth-Heinemann: Oxford, 1997.

phases. This orientation corresponds to the (minimal) cusp at the γ-plot.

In the neighborhood of a minimal γ_{cs} (denoted by γ_{cs}^{min}), $\gamma_{cs}(\alpha)$ is given by[25]

$$\gamma_{cs}(\alpha) \approx \gamma_{cs}^{min} + \frac{\epsilon b \varphi}{4\pi(1-\nu)}\left(1 - \frac{\varphi - \varphi_{max}}{\varphi_{max}}\right) \quad (26)$$

where γ_{cs}^{min} = minimal specific interfacial free energy at a given orientation α, ϵ = elastic modulus, υ = Poisson constant, b = Burgers vector, φ = misorientation angle.

Combining eqs 8 and 26 yields

$$m \approx \frac{\gamma_{sf}}{\gamma_{cf}}\left\{1 - \frac{1}{\gamma_{sf}}\left[\gamma_{cs}^{min} + \frac{\epsilon b \varphi}{4\pi(1-\nu)}\left(1 - \frac{\varphi - \varphi_{max}}{\varphi_{max}}\right)\right]\right\} \quad (27)$$

Obviously, an excellent structural match ($\gamma_{cs}(\alpha) \rightarrow 0$, at $\varphi \rightarrow 0$) between the nucleating phase and the substrate leads to $m \rightarrow \gamma_{sf}/\gamma_{cf}$. In the case where $\gamma_{sf} \approx \gamma_{cf}$, one has then $m \rightarrow 1$, and $f(m) \rightarrow 0$ (cf. eq 19). This implies that ΔG_{heter}^{*} almost vanishes completely (cf. eq 6). This occurs only when the growth of the crystals is well orientated and ordered with respect to the structure of the substrate. In this case, the excellent epitaxial relation arises.

As the structural match varies from a perfect to a poor match, m decreases from 1 to 0, -1. The extreme case will be $m \rightarrow -1$, corresponding to the situation where the crystal−substrate correlation (interaction and structural match between nuclei and the substrate) does not exist. This is the case where substrates exert almost no influence on nucleation (the vanishing of the epitaxial effect), and nucleation is controlled by the homogeneous nucleation kinetics. Nuclei emerging in this case are completely disordered, bearing on correlation to the substrate. One has then $f(m,R') = 1$.

In general, as $f(m,R')$ varies from 0 to 1 (or m from 1 to -1), the interfacial structural correlation between the nucleating phase and the substrate changes from a completely correlated and interfacial structure ordered state to a completely uncorrelated and disordered state.

Due to the anisotropy of the crystalline phase, the deviations from the optimal structural match position toward the secondary optimal structural match (the second-lowest $\gamma_{cs}(\alpha)$) will adopt discrete values, which will first be the second-lowest minimum of γ_{cs} in the orientation of $\{h'k'l'\}$. A similar principle holds for further deviations. Therefore, according to eq 27, the deviation from the optimal structural match reflects the transition of m from m_1 to lower and discrete values $m = m_2, m_3$, and so forth.

Kinetically, the occurrence of substrates will, on one hand, lower the nucleation barrier, resulting in an increase in the nucleation rate, and on the other hand, exert also a negative impact on the surface integration. The substrates on which nucleation takes place will reduce the effective collision of structural units to the surface of clusters, where the structural units are incorporated into the crystal phase. This effect, similar to the effect of shadow, will slow the nucleation kinetics, in contrast to the lowering of the nucleation barrier. *This negative shadow effect* is described by $f''(m)$ and $f(m)$ appearing in the preexponential term of eq 20.

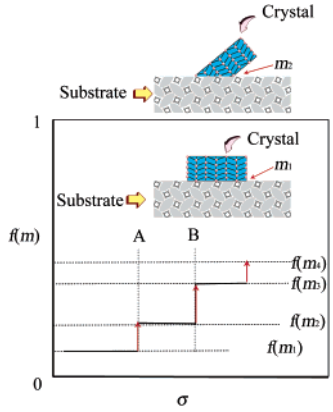

Figure 2. Illustration for supersaturation-driven interfacial structural mismatch: with the increase of supersaturation, the interfacial correlation factor $f(m)$ will increase abruptly at certain supersaturations, such A, B, ..., corresponding to the transition from an ordered and structurally matched to a less ordered and structurally mismatched biomineral/substrate interface. $m_1 > m_2 > m_3 > m_4$.

These two contradictory effects play different roles in different regimes. At low supersaturations, the nucleation barrier is very high (cf. eq 1). The nucleation rate will be substantially enhanced if the nucleation barrier is suppressed effectively ($f(m) \rightarrow 0$). Therefore, the heterogeneous nucleation with a strong interaction and an optimal structural match between the substrate and the nucleating phase ($m \rightarrow 1$) will be kinetically favored. In this case, the nucleation of crystalline materials will be best templated by substrates having an excellent structural correlation with the crystalline phase. The structural synergy between the crystalline materials (or biominerals) and the substrates will be optimal in this regime.

Nevertheless, the templating relation between substrates and crystalline materials is not always achievable even for the substrates having the optimal structural match with crystalline materials. At higher supersaturations, the exponential term associated with the nucleation barrier becomes less important. Instead, the issue of effective collisions or *the shadow effect*, described by the preexponential factors $f(m)$ and $f''(m)$, becomes more dominant in controlling the kinetics. Nucleation on substrates having larger $f(m)$ and $f''(m)$ (or $m \rightarrow 0, -1$, meaning the weak interaction and poor structural match between the substrate and the nucleating phase) is kinetically more favorable. From the point of view of statistical physics, this implies a lower degree of restriction from the substrate and a higher degree of orientational freedom (or a larger entropy.)

It follows from the above analysis that if σ progressively increases from low supersaturations to high supersaturations, nucleation will be governed by a sequence of heterogeneous processes associated with progressively increasing $f(m)$. Since for a crystalline phase, m and $f(m)$ adopt only values which correspond to some crystallographically prudential orientations, $f(m)$ will also adopt some increasing discrete values as σ increases.

On the basis of this principle, it can be seen that the quantity $f(m)$ describing the interfacial correlation between biominerals

(22) Kashchiev, D. In *Science and Technology of Crystal Growth*; van der Eerden, J. P., Bruinsma, O. S. L., Eds.; Kluwer Academic Publ.: Dordrecht, 1995; pp 53−66.
(23) Mutaftschiev, B. In *Handbook on Crystal Growth*; Hurle, D. T. J., Ed.; North-Holland: Amsterdam, 1993; pp 187−220.
(24) Liu, X. Y. In *Advances Crystal Growth Research*; Sato, K., Nakajima, K., Furukawa, Y., Eds.; Elsevier: Amsterdam, 2002. To be published.
(25) Gebhardt, M. In *Crystal Growth: An Introduction*; Hartman, P., Ed.; North-Holland: Amsterdam, 1972; pp 105−142.

and substrates will increase with supersaturation, as illustrated in Figure 2. This implies that the increase of supersaturation will drive the substrates/biominerals from an interfacial structural match state (a lower $f(m)$) to a state of higher mismatch (a higher $f(m)$). This phenomenon is referred to as *supersaturation-driven interfacial structural mismatch.* As mentioned above, the changes from one state to the other occur abruptly at certain supersaturations (such as A, B, ... in Figure 2) due to the anisotropy of the crystalline phase.

Experimental Section

As mentioned in the previous section, the kinetics of nucleation can be examined on the basis of the correlation between the nucleation induction time and supersaturation (cf. eq 24). Due to the crystallization sequence, what we normally measure is the induction time t_i in crystallization, which is defined as the mean time elapsing before appearance of an observable amount of the new phase. Actually, t_i includes the time t_g for the growth of crystals to the observable size and the induction time for nucleation t_{nucl}. Within t_{nucl}, there is certain time required to establish nucleation from time zero to the steady state.[20−24] This is the transient period t_{nonst}, which is associated with nucleation of the nonstationary state. In addition, t_{nucl} should also include t_s. It follows then that

$$t_i = t_g + t_{nonst} + t_s \tag{28}$$

Since the free energy barrier for three-dimensional nucleation is much higher than that in two-dimensional nucleation,[12,24] the growth of crystals is in most cases much easier than nucleation. If crystals with a sufficiently small size can be detected by certain techniques, we then can have $t_g \ll t_{nucl}$ ($= t_{nonst} + t_s$). At the present time, the laser light-scattering method promises the detection of particles from several nm to several tens of nm. This has already been very close to the critical size of nuclei in many cases. In such a situation, we can even assume $t_g \rightarrow 0$.

Apart from this, t_{nonst}, according to the previous section, is determined to a large extent by the diffusivity of nucleating species. If the mother phase is not too viscous, such as aqueous solutions, we normally have t_{nonst} equal to a few microseconds.[19,20] This implies that $t_{nonst} \ll t_s$. Therefore, we can approximate eq 28 by

$$t_i \cong t_{nucl} \cong t_s \tag{29}$$

In other words, this implies that under normal condition, the nucleation rate J is time-independent.

Notice that, since the nucleation rate is inversely proportional to the induction time and the volume (cf eq 23) in applying eq 24 to study the nucleation kinetics, V should be kept constant in a given condition if we wish to find the direct correlation between the nucleation rate and the induction time. This can be an important step to gain a set of consistent and reproducible data.

We will examine the nucleation kinetics of biominerals from solution using a newly developed advanced fast dynamic light-scattering method (FDLS),[26,27] based on a Brookhaven BI-200SM light-scattering system with a He−Ne laser (632.8 nm) source and a photomultiplier tube (PMT) detector. The system can detect particles of size down to 2−4 nm, which allows an in situ measurement of the nucleation process and of the size increase of the nuclei. To obtain a fundamental understanding, the experiments were carried out under both gravity and microgravity.

In the experiments of $CaCO_3$, the ionic strength is fixed at 0.11 M. The experiments were carried out in a stopped-flow system at $T =$ 297 K and pH = 6.3−7.3. Before carrying out the experiments, the nucleation vessels were cleaned properly, and the solutions were filtrated several times by filters with a pore size of 220 nm. The nucleation kinetics was examined by measuring the induction time of nucleation at different supersaturations.

The $CaCl_2$ and Na_2CO_3 solutions were mixed and introduced into a rectangular glass cell ($10 \times 10 \times 44$ mm^3) via a stopped-flow system.[26,27] Both solutions contain 1 mg/mL type I collagen. The system allows uniform mixing of the two solutions within about 20 ms. The measurement of the induction time t_s started immediately after the two solutions were mixed. The light-scattering shows that the solution flow after filling the solution from the stopped-flow cell vanishes completely in less than 1 s, which is much shorter than t_s, and therefore exerts no effect on t_s measurement. This experimental setup allows sufficient time for rapid measurement, giving rise to good reproducibility[26,27] The X-ray diffraction (XRD) analyses showed that $CaCO_3$ samples obtained under the above conditions are mainly calcite.

Similarly, HAP precipitates were obtained by mixing calcium nitrate 4-hydrate $Ca(NO_3)_2{\cdot}4H_2O$ (>99.9%, pro analysis, Merck) and di-ammonium hydrogen phosphate $(NH_4)_2HPO_4$ (>99% Merck), solutions. The ratio of Ca/P in HAP is 1.67, hence the mole ratio of $Ca(NO_3)_2{\cdot}4H_2O$ and $(NH_4)_2HPO_4$ was adjusted to be 1.67. The pH of the reacting solutions was adjusted at about 10 using NH_3(aq) to ensure that the precipitation resulting from the reaction is the desired HAP structure, excluding polymorphs, such as calcium hydrogen phosphate 2-hydrate (brushite), $CaHPO_4{\cdot}2H_2O$. The X-ray diffraction (XRD) analyses for the samples prepared under such conditions were carried out, and the obtained XRD pattern matches that of HAP crystals from the International powder diffraction file.

To examine the effect of microgravity on biomineralization, we also examined the nucleation of $CaCO_3$ in microgravity. The experimental conditions are the same as those in gravity. To create the microgravity environment, an MU-300 double-jet airplane was used to attain a 20-s microgravity condition during a parabolic flight. For more experimental details, see refs 26 and 27.

Results and Discussion

Biomineralization under the Influence of Substrate and Supersaturation. The concrete evidence supporting the above analyses can be identified from the $\ln(t_s) \approx 1/[\ln(1+\sigma)]^2$ plot. According to eq 24, the plot of $\ln(t_s) \approx 1/[\ln(1+\sigma)]^2$ will give rise to a straight line whose slope is determined by κ and $f(m)$. Obviously, for a given system (κ, $B' =$ const), the slope of the straight line will change accordingly to $f(m)$. In this sense, the slope of the $\ln(t_s) \approx 1/[\ln(1+\sigma)]^2$ plot gives the relative $f(m)$ for the system. Therefore, one can analyze the change of the correlation between the substrate and the crystalline phase in terms of the variation of the slope.

For $CaCO_3$, plotting $\ln(t_s)$ versus $1/[\ln(1+\sigma)]^2$ within a range of supersaturations obtains a curve, which can be in principle fitted by three pairwise intercepting straight lines of different slopes, partitioning the space into three regimes. (See Figure 3a). The occurrence of three straight lines with different slopes indicates that the nucleation is controlled by three discrete values of $f(m)$ within three supersaturation regimes. Considering that supersaturation increases progressively from Regime I to III in the case of $CaCO_3$ (cf. Figure 3a,b), if we denote $f(m)$ in these three regions as $f(m_1)$, $f(m_2)$, $f(m_3)$, respectively, we should have then $f(m_1) < f(m_2) < f(m_3)$ due to the supersaturation-driven interfacial structural mismatch. This is exactly what we have obtained for $CaCO_3$ (see Figure 3b). The result is in very good agreement with the predicted changes shown in Figure 2.

(26) Tsukamoto, K.; Maruyama, S.; Shimizu, K.; Kawasaki H.; Morita, T. S. In Microgravity. *Parabolic Flight* **1997**, *7*, 51−57.
(27) Tsukamoto, K. *Extended Abstract of AIST Workshop*; Hokkaido, 1998; p 29−33. Liu, X. Y.; Tsukamoto, K.; Soral, M. *Langmuir* **2000**, *16*, 5499−5502. Liu, X. Y. *Appl. Phys. Lett.* **2001**, *79*, 3539−3542; *J. Chem. Phys.* **2001**, *115*, 9970−9974.

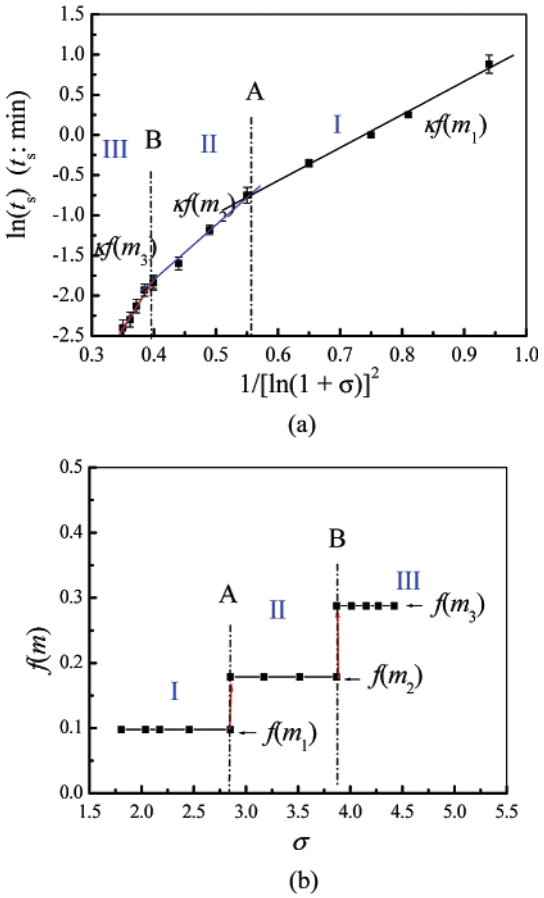

Figure 3. (a) Plot of ln t_s vs $1/[\ln(1+\sigma)]^2$. Three straight lines of different slopes intercept with each other, dividing the space into three regimes. (b) Experimental verification for *the supersaturation-driven interfacial structure mismatch* (cf. Figure 5.) $f(m)$ is obtained on the basis of the fact that under microgravity, $f(m_{\mu g}) = 1$, $f(m_{\mu g})\kappa = \kappa = 42$ (cf. Figure 6). Under gravity, $f(m) =$ Slope $[f(m)\kappa]/\kappa$.

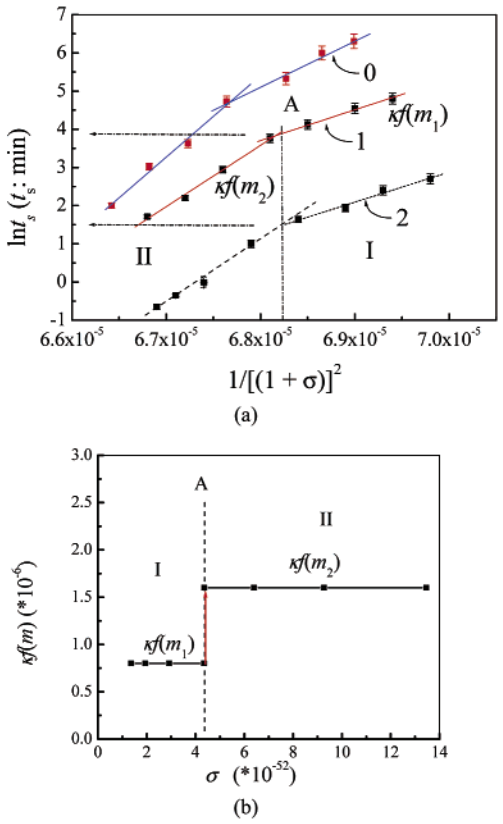

Figure 4. (a) Plot of ln t_s vs $1/[\ln(1+\sigma)]^2$. For each set of data, two straight lines of different slopes intercept with each other, dividing the space into two regimes. Curve 0: 0 collagen; Curve 1: 1 mg/mL collagen; Curve 2: 10 mg/mL collagen. (b) Experimental verification for the supersaturation-driven interfacial structure mismatch (cf. Figure 3): The step increase of $f(m)$ with supersaturation for Curves 1 and 2 in (a).

Similar results were obtained for HAP (see Figure 4). The main characteristics of HAP nucleation are the same as $CaCO_3$. The only difference is that within the given range of supersaturation, only two heterogeneous nucleation regimes (Regimes I and II) were identified.

Notice that in Figure 4a, Curve 0 describes the nucleation kinetics of HAP under the influence of dust (foreign particles) in the solutions (the collagen concentration is equal to 0), whereas Curves 1 and 2 describe that under the influence of collagen (the collagen concentrations are 1 and 10 mg/mL, respectively). The kinetics described by Curve 0 is obviously very much different from that by Curves 1 and 2 where collagen is added. Comparing Curve 0 with Curves 1 and 2, one can see that the slope of the corresponding straight line in Curve 0 is much higher than those in sets 1 and 2. This implies that collagen fibers are much more effective in lowering the nucleation barrier of HAP than foreign particles. Apart from this, the corresponding $\ln(t_s) \approx 1/[\ln(1+\sigma)]^2$ plots of Curves 1 and 2 shift further downward than Curve 0, meaning that collagen fibers serve much better as templates than normal foreign particles.

Since collagen fibers serve as "seeds" for HAP nucleation, the change of the collagen concentration is equivalent to the change of $N°$ in eqs 20 and 24. This, according to eq 24, will lead to a parallel shift of the plot of $\ln t_s \approx 1/[\ln(1+\sigma)]^2$ by $\ln N°$ along the y direction. On the basis of eq 24, we should expect a parallel downward shift of two lines in Curve 1 by a value of 2.3 (ln 10) after increasing the collagen concentration for 10 times. This is verified by our experiments as shown in Figure 4a, where a shift of 2.4 is obtained. As a consequence, the transition from Regime I to II occurs at the same supersaturation (A). Similar to Figure 3b, the supersaturation-driven structure mismatch of HAP for the occurrence of collagen is described in terms of $f(m)$ in Figure 4b.

The nature of nucleation may determine the structural synergy between biosubstrates (including biomineral crystallites[18]) and biominerals and consequently the basic structure of hard tissues or teeth. If nucleation proceeds in a heterogeneous manner, a strong interaction between the nucleating phase and the substrate is expected. In this case, the adherence of biominerals to the substrates will be strong, and the structure of hard tissue should be compact and tough. Conversely, if the substrates exert no impact on nucleation, nucleation will occur randomly in the bulk of the fluid phase. This will significantly reduce the adherence and the structure synergy between the substrates and biominerals. On the basis of this principle, the above templating and the contradictory supersaturation-driven interfacial structure mismatch effects may have important implications for biomineralization in biological systems.

At low supersaturations, the nucleation barrier is very high (cf. eqs 1 and 3). The nucleation rate will be substantially enhanced if the nucleation barrier is lowered. Therefore, the

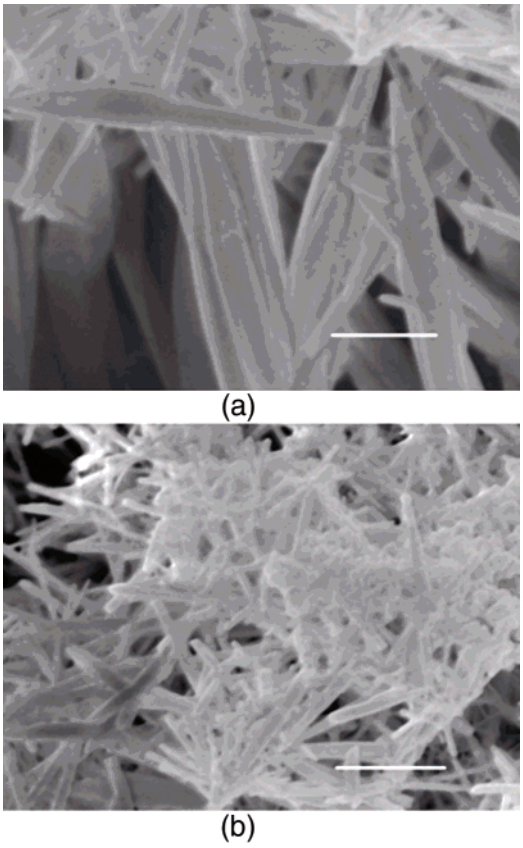

Figure 5. (a) SEM micrograph shows compact HAP crystals obtained from a relatively low supersaturation in Regime I (cf. Figure 4). Due to the template effect of biosubstrate, the crystallites show a very good structural synergy. Biomineralization in this regime could lead to an ordered, compact, and tough structure. (b) At high supersaturations, *supersaturation will result in the interfacial structural mismatch* between biominerals and biosubstrates, resulting in a less ordered, porous, and loose structure. The SEM micrograph shows open and porous HAP crystals obtained from a relatively high supersaturation in Regime II (cf. Figure 4). Scale bars: 500 nm. The crystals were filtered and washed by acetone before examination by SEM.

heterogeneous nucleation accompanied by a small $f(m)$ (implying a strong interaction and a very good structural match between biosubstrate (existing HAP crystallites) and nucleating Ca minerals) will be kinetically favored.

In this case, resulted biomineral crystals will be compact and ordered. (See Figure 5a.) Therefore, hard tissues resulting from biomineralization under such a condition could become tough and compact.

Conversely, at higher supersaturations, due to the effect of the supersaturation-driven interfacial structure mismatch, nucleation on the substrates (HAP crystallites) adopts a larger $f(m)$ and $f''(m)$ (implying a weak interaction and a poor structural match between biosubstrate and nucleating Ca minerals). In this case, biomineral crystal aggregates obtained will be open and porous. (See Figure 5b.) In this case, we may then obtain porous and brittle tissues.

The effect of fluorine (F) agents and supplements on the essential structure of children's teeth could also be understood on the basis of the above principle. In the period of dental mineralization, the nucleation of HAP under the influence of biosubstrates will determine the basic structure of the teeth. The occurrence of F will significantly reduce the solubility of Ca phosphate minerals and therefore considerably enhance the

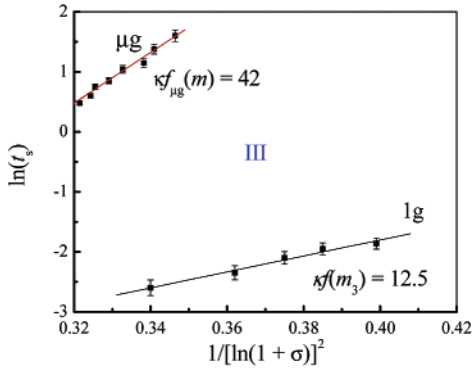

Figure 6. Plot of ln t_s vs $1/[\ln(1 + s)]^2$ under both gravity and microgravity. The slope of ln t_s vs $1/[\ln(1 + s)]^2$ plot under microgravity is a factor 4 larger than that obtained from the gravity experiments. Due to the nature of homogeneous nucleation, under microgravity $f(m_{\mu g}) = 1$, $f(m_{\mu g})k = k = 42$.

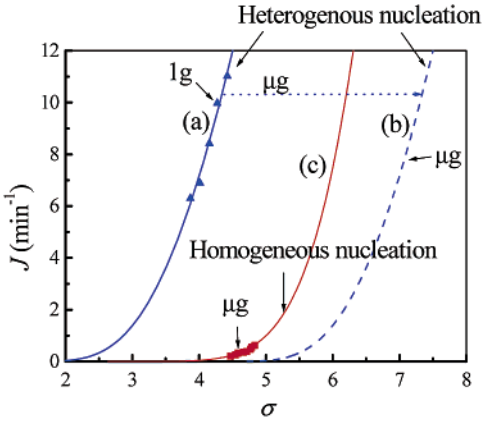

Figure 7. Relative nucleation rate J plotted vs supersaturation s for $CaCO_3$ under gravity (1 g) and microgravity (μg). (▲) Experimental data measured under gravity; (■) experimental data measured under microgravity. (Curve a) Nucleation rate as a function of supersaturation s according to the heterogeneous nucleation mechanism. (Curve c) Nucleation rate as a function of supersaturation s according to the homogeneous nucleation mechanism. Under gravity, heterogeneous nucleation occurs much faster than heterogeneous nucleation within the given supersaturation range. (Curve b) Under microgravity, due to the lack of convection, a drop in the effective surface supersaturation around biosubstrate occurs. To reach a nucleation rate similar to that under gravity, a much higher bulk supersaturation is required. This leads to the fact that the kinetics of heterogeneous nucleation on biosubstrate will shift from Curve a to Curve b. On the other hand, gravity has almost no effect on homogeneous nucleation. Consequently, the homogeneous nucleation becomes more kinetically favorable than heterogeneous nucleation. Therefore, the homogeneous nucleation rate becomes measurable.

supersaturation for biomeralization.[4] Due to the effect of the supersaturation-driven interfacial structure mismatch, the formation of a porous structure of teeth may occur.

Microgravity-Driven Homogeneous Nucleation and the Effect on Biomineralization. The kinetics of $CaCO_3$ nucleations under gravity and microgravity are shown in Figures 6 and 7. The variation of supersaturation is limited within Regime III of Figure 3. It is surprising to see that in microgravity, the line of $\ln(t_s) \approx 1/[\ln(1 + \sigma)]^2$ has a slope of 42, which is almost 4 times larger than that obtained in gravity within the same supersaturation regime (cf. Figure 6). This implies that $[f(m)]_{III}$ is not the highest and that the nucleation of $CaCO_3$ in Regime III of Figure 3a is still controlled by heterogeneous nucleation rather than by homogeneous nucleation. Assuming that the nucleation occurring in microgravity belongs to homogeneous nucleation, the slope of $\ln(t_s) \approx 1/[\ln(1 + \sigma)]^2$ plot by taking

$f(m) = 1$ gives rise to the interfacial free energy of 170 mJ/m^2 at 25 °C (cf. eqs 24 and 25). This is almost the same as the estimated $CaCO_3$ crystal surface energy from the contact angle measurements.[28] This result strongly suggests the occurrence of homogeneous nucleation in microgravity.

The microgravity effect can be understood in terms of convection. It is well-known[9,20] that convection does not exert a large influence on the diffusion field around tiny particles highly dispersed in the bulk phase, such as clusters. This is the case for homogeneous nucleation. On the other hand, nucleation on a substrate will be very different. Like a sink, each nucleus will create its own diffusion field on the surface of the substrate. When the neighboring diffusion fields overlap, the concentration depletion occurs at the surface. Then convention will to a large extent compensate for the depletion. This implies that convection has a direct impact on heterogeneous nucleation but no impact on homogeneous nucleation.

In gravity, convection, due to a temperature or a concentration gradient caused by nucleation, will help to transport growth units from the bulk to the surface of the substrates. This will compensate for the concentration (or supersaturation) depletion during nucleation at the surface of the substrates so that the effective supersaturation at the surface of substrates is approximately the same as the bulk supersaturation. In this case, homogeneous nucleation is not kinetically favorable (see Figure 7). Under microgravity, however, the convection owing to the temperature or concentration gradient is suppressed. It was shown in our experiments that gravitational sinks caused by the convection of the solution, which is the upstream convection plume caused by gravity leading to an inhomogeneity in the scattering image, are very prominent in gravity and have an average diameter of 600 nm.[26,27] The gravitational sinks disappear soon after microgravity is introduced,[26,27] and the image obtained in microgravity is much more uniform. This indicates that the convection is eliminated in microgravity. As a consequence, microgravity will significantly slow the transport of growth units toward the substrate surface, causing a depletion of concentration and supersaturation during the nucleation on the substrates. To achieve the nucleation rate for heterogeneous nucleation ($f(m) \ll 1$) similar to that under gravity, much higher bulk supersaturations are required. (See Curves a and b in Figure 7.) *On the other hand, microgravity has almost no effect on homogeneous nucleation. Homogeneous nucleation* ($f(m) = 1$) *may be achieved more easily.* (See Figure 7.) Therefore, *microgravity considerably suppressed heterogeneous nucleation so that homogeneous nucleation may be achieved more easily*.

As mentioned before, in the case of heterogeneous nucleation ($f(m) \ll 1$), the coherence and structural match between Ca minerals and biosubstrates are very good due to the nature of this type of nucleation. This may lead to a more compact and tough structure of hard tissue. In the case of homogeneous nucleation ($f(m) = 1$), there is no coherence or structural match between Ca minerals and biosubstrates. This could lead to a very porous and brittle structure of hard tissue, and microgravity-induced osteoporousis.

Acknowledgment. The work is supported by Project R-144-000-076-112/432/650.

JA020355D

(28) Tsukamoto, K. To be published.